# Mechanical Properties of Superconducting Materials


**Essia Hannachi and Yassine Slimani**

**Abstract** Superconducting materials are currently the key research target in the field of basic and applied superconductivity. The intrinsic brittleness and the poor mechanical properties of several superconductors such A15 alloys, high $T_c$ superconductors (HTSc) and non-cuprates superconductors, halt in the pathway of a broad extent of actual applications. In order to be better commercialized, some factors have to be controlled and optimized among which is the development of exceptional processing methods for fabrication of usable superconductors. This book chapter examines the up-to-date of mechanical characteristics of superconducting materials. We start by giving an overview of the different testers used for measuring the mechanical behavior. One of the most significant mechanical properties to be enhanced is the microhardness. Therefore, we focused in the next section to microhardness and various models adopted to analyze it. Also, the mechanical nature of different types discovered superconductors from alloys, cuprates, to non-cuprates has been deeply reviewed and discussed. For each case, challenges and recent results for getting commercialized superconductors material with good mechanical properties were presented.

**Keywords** Superconductor · Mechanical · Microhardness · Stress–strain · Commercialization

## 1 Introduction

Superconducting materials have huge potential to bring about drastic revolutions in electric power and giant-field magnet technology and, allowing high-capability

E. Hannachi (✉)
Department of Nuclear Medicine Research, Institute for Research & Medical Consultations (IRMC), Imam Abdulrahman Bin Faisal University, P.O. Box 1982, Dammam 31441, Saudi Arabia

Y. Slimani
Department of Biophysics, Institute for Research & Medical Consultations (IRMC), Imam Abdulrahman Bin Faisal University, P.O. Box 1982, Dammam 31441, Saudi Arabia
e-mail: yaslimani@iau.edu.sa



Y. Slimani and E. Hannachi (eds.), *Superconducting Materials*,
https://doi.org/10.1007/978-981-19-1211-5_4

dissipation-lower transmission of electric power, high-productivity electric power generation, ultra-high magnetic field production for magnetic resonance imaging (MRI) systems with good resolution, tiny lightweight electrical apparatus, high-speed maglev transportation, nuclear fusion reactors, nuclear magnetic resonance (NMR), and imminent progressive extreme energy particle accelerators, etc. The economy, functioning, and operational parameters (magnetic fields and temperatures) of these applications intensely dependent on the mechanical and electromagnetic characteristics, as well as the production and price of materials. The mechanical performance of superconducting materials has been of relevance and concern to researchers in this field. The brittleness inherent in several high-field superconductors needs the development of unique processing techniques for manufacture of usable conductors. Fundamental investigations of the influences of mechanical stress on superconducting characteristics offer a deep insight into the nature of superconductors. In last years, attention in the mechanical comportment of commercialized superconductors has increased due to the great mechanical forces anticipated in projected superconducting devices like energy storage, rotating machines, magnets for plasma confinement and, and electrical transmission lines [1–3]. In many laboratories located around the world, equipment for examining the mechanical properties of superconducting materials has been developed. Results from these measurements have become more accessible over the past years; Thus, it is exciting to examine the mechanical behavior and impacts of stress in superconducting materials. The assessment of mechanical properties led to distinguish and enhance the permanence of traditional devices. This chapter will review the mechanical properties of superconducting alloys and compounds at ambient and low temperatures, the stress effects on superconducting characteristics, and their implications for superconducting applications.

## 2 Mechanical Properties Measurements

The Mechanical features of superconducting materials are fully linked to other including electrical, structural, and physical characteristics to establish the devices execution. The mechanical characteristics of the material are usually measured by hardness test, compression tests and tensile tests, bending test.

### *2.1 Hardness Test (HT)*

HT is the most general test that is employed to assess mechanical characteristics. Hardness is defined as the capacity of one material to scratch another material or the resistance to indentation. The indentation hardness is the most usually employed form of hardness. Conical, pyramidal, or spherical indenters have been employed for the indentation hardness tests. There are three main standard test methods for

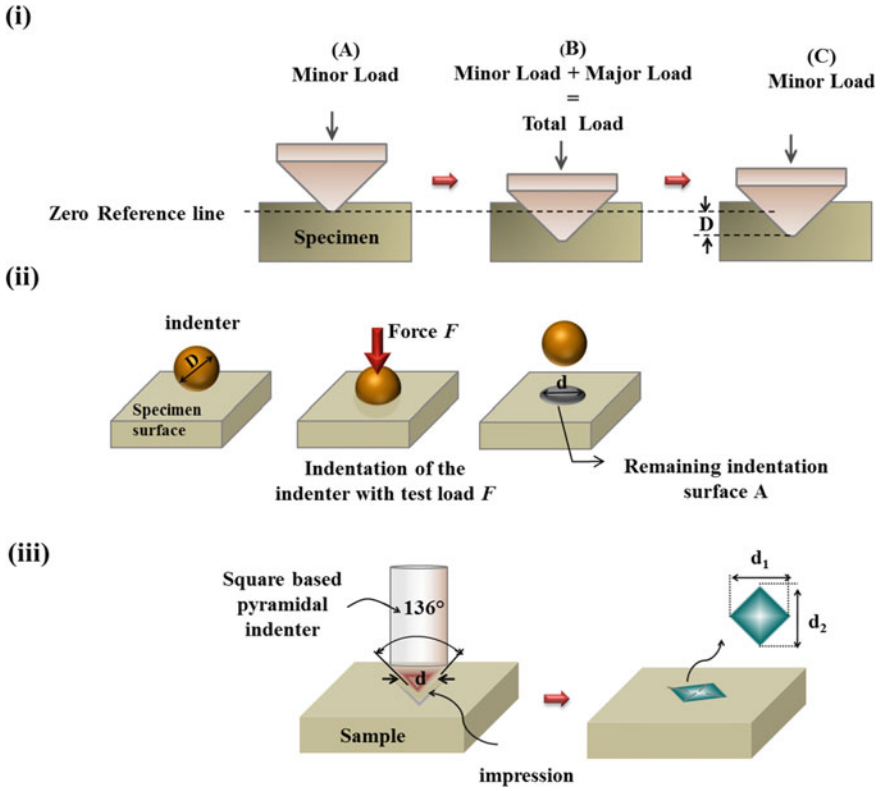


**Fig. 1** (i) Rockwell hardness testing, (ii) Brinell hardness testing, and (iii) Vickers hardness testing

manifesting the correlation between hardness and impression size: Brinell, Vickers, and Rockwell (Fig. 1).

The HT have certain benefits and disadvantages. For instance, no scale, in the simplest and most widely employed indentation hardness, Rockwell hardness, extends sufficiently to the full range of materials used to make sheet metal. Also, each thickness gauge has the minimum required to avoid the effect of the anvil, i.e. the effect of the outrigger or support on the observed hardness. The benefits of indentation hardness techniques are that they are less destructive, fast, and can be applied to small material samples and localized materials in fashion.

## *2.2 Compression Test (CT) and Tensile Test (TT)*

Compression test (CT) includes a specimen of the material having dimensions defined by the proper standard by carrying two pressure plates together to press the sample. Special procedures require material cylinder pressure but the particular material

shape can change depending on the normal protocol. The exerted force and cross shift data are amassed in real time and the test goes on till the specimen flops or the tester selects to terminate the test. The CT can give the yield strength, ultimate compressive strength, modulus of elasticity and hardness of the sample. The TT is the most extensively employed test in controlling the mechanical characteristics of the materials. In TT, a particularly fabricated sample is exposed to steadily rising uniaxial tension force. The material elongation is measured instantaneously. The measurement via TT yields to curves of the engineering strain and stress. The engineering strain and stress are given by the following expressions, respectively [4]:

$$S = P/A_0 \tag{1}$$

$$e = \Delta l/l_0 \tag{2}$$

where $A_0$ is the initial cross-section sample area, $\Delta l$ is the variation in length, and $l_0$ is the original length of the sample. At the start of the test, the material stretches flexibly, and if the load is released, the specimen returns to its original length. The material is said to have exceeded elastic limit 3 when the load is enough to begin a plastic or non-recoverable deformation. On additional loading, the stress due to continuous plastic deformation increases with increasing plastic stress, i.e., the hardening of the metallic strain. Compression is reached at maximum tensile strength. At this point the embedding initiates and the engineering stress declines with more pressure until the material breaks down.

The engineering strain–stress curves does not provide a correct clue of the deformation properties of a material since it is based on the primary sample dimensions. Yet, the dimensions of the sample vary uninterruptedly during the test. If the stress is measured from the instant cross-sectional area related to a special load rather than the original stress, then it is named the true stress σ. The true stress is termed as the ratio of the load of the specimen $A_i$ to the instant least cross-sectional area reinforcing that load $w$.

The true strain $\varepsilon$ is given by [4]:

$$\varepsilon = \ln\left(\frac{l_i}{l_0}\right) \tag{3}$$

Here $l_0$ is the original length and $l_i$ the instant length. The tensile tests have some limitations. They are usually time expending, destructive and necessitate particularly prepared samples.

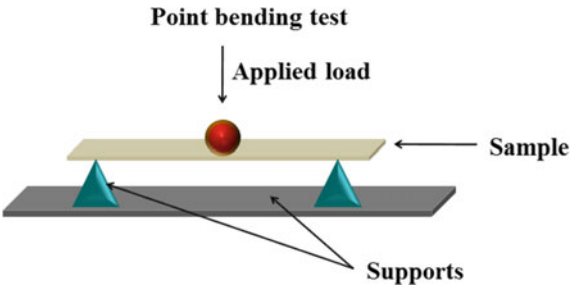


**Fig. 2** 3-Point bending test method. three-point bending delivers three points of contact; dual supports and one center point where the loading is applied

## *2.3 Three-Point Bending Tests*

Bending tests (BT) are usually performed to control the mechanical characteristics of the material like ductility, bend strength, fracture strength of the material to fracture. BT distort the test material at its midpoint allowing it to form a concave or bend surface without fracture with a particular radius of curvature (Fig. 2). There are four known kinds of BT. In a guided BT, the specimen is positioned horizontally via two supports and after that a force exerted to the top of the midpoint distorting the specimen into a "U" form. In a semi-guided BT, the midpoint of the specimen is bent at a certain angle or internal radius. In a free BT, the extremities of the specimen are pushed together, without any application of the force to the bend itself. Finally, ASTM E399; the common fracture toughness tester which consists of a specimen with a pre-cracked initial crack on the underside of the midpoint that is loaded into a three-point bending point such that midpoint force is applied to the opposite face of the fracture. 3-point bending tests provide information about the flexural stress, flexural strain of bending, and elastic modulus a material. Hard materials like high temperature superconductors can be analyzed by means of BT as a gauge of the material in both compression (the top of the material as it is tested) and tension (the bottom side of the specimen as it is tested).

## *2.4 Instrumented Indentation*

Indentation testing is a useful technique that is based principally on the contact between the material of concern, whose mechanical characteristics like hardness, elastic modulus are unidentified, with another material, whose characteristics are identified [5]. The technology's origins date back to the 1822 Mohs hardness scale, in which material capable of leaving a lasting abrasion in another material were classified as harder, with diamonds designated a value of 10 on the scale as a maximum. The creation of Vickers, Brinell, Rockwell and Knoop testing comes from an improvement in the indentation test method, in which the penetration length scale is measured in nanometer scale instead of millimeters or microns, the latter being frequent in traditional HT. Aside from the displacement scale included, the hallmark of the majority

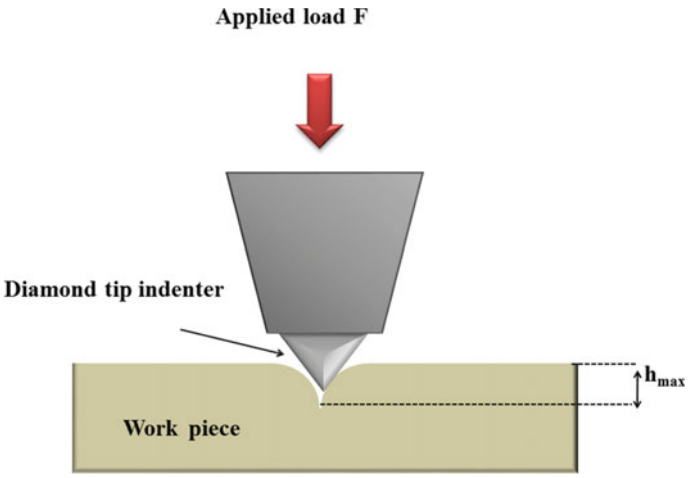


**Fig. 3** Schematic illustration of nano indentation test

nanoscale indentation tests is the indirect measurement of the contact area. In traditional HT, the contact area is determined from direct measurements of the extents of the impression remaining in the sample's surface when the load is removed. In nanoscale indentation tests, the residual impression size is on the order of microns and too miniature to be opportunely measured directly. Consequently, it is common to determine the contact area by computing the depth of the indentation mark in the sample of concern. Figure 3 illustrates schematic depiction of nano indentation test. This, along with the known indenter geometry, offers an indirect measurement of the contact area at filled load. For this purpose, nano indentation can be deemed as a particular case of instrumented indentation test or depth sensing indentation. Nano indentation has been extensively employed for describing the mechanical properties of nano materials [6], and thin film [7], due to its exalted sensitivity and the outstanding resolution for getting the nano hardness, elastic modulus and the plastic/elastic deformation behaviors in a quite simpler mode. Over a nano indentation test, a diamond tip is compressed into the sample till a specified extreme load or depth is attained and then the load is detached. Instantaneously, the displacement of, as well as the load on, the indenter is registered. The results of instrumented indentation deliver evidence about the mechanical characteristics of the material, involving hardness, plastic deformation and elastic moduli. One main parameter of indentation test is that the tip requires to be monitored by displacement or force that could be measured instantaneously in the indentation cycle [8]. Some of the usually measured mechanical characteristics include the hardness, the ultimate tensile strength, the Young's modulus yield strength, and work hardening coefficients. The mechanical characteristics offer evidence on the strength and for the specification of materials.

## 3 Microhardness and Models

Microhardness is the hardness of a material as defining by forcing an indenter such as a Vickers or Knoop onto the material's surface under a load from 15 to 1000 gf; frequently, the indents are so tiny that they need to be measured with a microscope. The frequently checked static process HT entails applying a static load to an indenter of diamond and measuring, by means of microscope, the transverse indentation size on the sample surface after unloading. The most commonly employed form of indenter geometry, the angle of a diamond pyramid with a square base between the opposite facades of the pyramid is 136° as the indent, which is the Vickers indenter [9]. On account of the shape the indenter is termed the diamond pyramid hardness (DPH) test [10]. Recently, Vickers microhardness testing has been utilized in numerous kinds of materials including ceramic, alloys superconductors, polymers, semiconductors, and thin films [11–15]. The microhardness of a material is dependent on the applied load [16, 17]. This fact is recognized as indentation size effect (*ISE*) behavior, elucidating the reduction in the hardness with the increase of the applied load. This comportment can result from diverse aspects such as plastic and elastic deformations, temperature, size of indentation, degree of voids/cracks and friction of the indenter [18]. The reverse of this phenomenon is known as reverse *ISE* (*RISE*) behavior, which explains the increase of microhardness as the applied load increases. As described above, the hardness is the most common test to examine the mechanical characteristics of a material since it is simple to operate, less destructive to the surface of the specimen. Other benefit of the hardness measurement allows to attain the supplementary parameters including brightness index, yield strength, fracture toughness, and elastic modulus.

The Vickers microhardness values ($H_V$) can be computed using to the conventional definition [19]:

$$H_V = 1854.4\left(\frac{F}{d^2}\right)(\text{GPa}) \tag{4}$$

$F$ is the applied load and $d$ is the indentation diagonal length. Many approaches have been used to analyze Vickers microhardness data.

### *3.1 Meyer's Theory*

The Meyer's concept is frequently employed measure of indentation hardness. Meyer proposed a power law empirical relation that correlates the load, $F$, and $d$ corresponding to the following Meyer's theory:

$$d^n = F/A \tag{5}$$

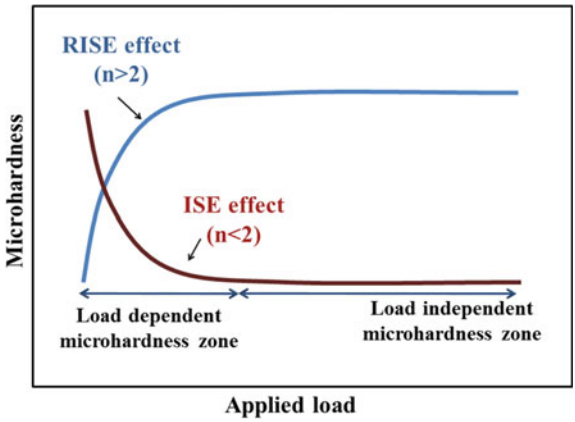


**Fig. 4** The variation of $H_v$ a function of applied load. $H_v$ decreases with increasing the applied load (ISE), whereas $H_v$ increases with increasing the applied load (RISE). For normal ISE, $n$ value <2, whereas for RISE, $n$ is >2

Here $A$ is a constant, representing the load needed to begin unit indentation. n is the Meyer's index, which defines the ISE. For normal ISE, $n$ value <2, whereas for RISE, $n$ is >2. If $n = 2$, $H_v$ is not dependent on the applied load (Fig. 4). Hence, ISE or RISE can be distinguished based on the obtained n values. So, Knowledge on the increment or decrement of microhardness with applied load can be identified.

## *3.2 Hays/Kendall Model*

In 1973, the model of energy losses has been predicted by Hays and Kendall [20]. This concept anticipated that there is a least test load $w$, named the specimen resistance pressure, which is compulsory to start plastic deformation, and further down it is merely elastic deformation happens. In another meaning, the indenter can enter the material beyond a particular value of load called the critical value of the applied load. Therefore, the size of the indentation begins to rise after the critical applied load value, and is proportionate to the effective load as $F_{eff} = F_{max} - W_{HK}$ rather than the applied load:

$$F_{\max} - W_{HK} = A_{HK} d^2 \tag{6}$$

$A_{HK}$ represents the hardness constant and it is applied load independent. From the plots of $F_{max}$ versus $d^2$, $W_{HK}$ and $A_{HK}$ are obtained. In addition, the subtraction $W_{HK}$ from the applied load, the true microhardness can be estimated as:

$$H_{HK} = 1854.4 \frac{F_{\max} - W_{HK}}{d^2} (\text{GPa}) \tag{7}$$

Therefore, the slope of the $F_{\max}$ versus $d^2$ gives $A_{HK}$ and $W_{HK}$ values. The positive value of $W_{HK}$ signifies that the material exhibits the ISE behavior while the

negative value of $W_{HK}$ indicates RISE feature for the sample. The positive value is enough to create the elastic and the plastic deformations in the material. The negative value signifies that the plastic deformation is dominant in the system [21].

### 3.3 Proportional Specimen Resistance (PSR) Model

PSR model was suggested by Li and Bradth [22] and is able to investigate the ISE behavior. This model contains the elastic resistance of the test specimen and the frictional effects at the indenter facet/specimen interface during micro indentation. According to PSR concept, the microhardness test load, $F$, and the resultant indentation size, $d$, showed to survey the following relation:

$$F = ad + bd^2 = ad + \left(\frac{F_c}{{d_0}^2}\right)d^2 \tag{8}$$

where the values of $a$ and $b$ are computed from the $F/d$ versus $d$ plots. The parameter $a$ typifies the load reliance of hardness. The value of the real microhardness is proportionate to $b$. Based on Li and Bradth analysis, $a$ and $b$ parameters can be correlated to the elastic and the plastic characteristics of the tested material, respectively. The ISE is a result of the relative resistance of the indentation size of the test specimen as defined by $a$. Whereas, b was found to be related to the load indentation that is non-reliant to hardness. It contains the critical indentation load, $F_c$, and the characteristic indentation size, $d_0$. Particularly, $b$ is proposed to be a gauge of what is termed "*true hardness*; $H_{PSR}$". For the micro indentation testing through a Vickers indenter, $H_{PSR}$ can be estimated directly from $b$ as [14]:

$$H_{PSR} = \frac{F - ad_0}{26.43{d_0}^2} = \frac{b}{26.43} \tag{9}$$

To confirm the validation of the PSR model in investigating the ISE, two series of the values of $H_{PSR}$ were used as: ${H_{PSR}}' = \frac{b}{26.43}$, and ${H_{PSR}}'' \frac{F-ad_0}{26.43{d_0}^2}$.

### 3.4 Modified PSR (MPSR) Model

MPSR model has been suggested by Gong and co-workers. [16] to study the ISE effect in different materials. The MPSR model was mainly introduced that the sample surface is generally subjected to a similar variety of stress triggered by automated processing and sample polishing [16]. This stress alters the resistance coefficient of the samples to $W = \alpha_0 + \alpha_1 d_0$, where $\alpha_0$ is related to the residual surface stress with negative low value and $\alpha_1$ with positive value so long as the lasting deformation is

formed. Bearing in mind these effects, Gong and co-workers proposed that the PSR approach could be revised as:

$$F = a + bd_0 + cd_0{}^2 \tag{10}$$

where $a$, $b$ and $c$ are experimental constants.$a$ is a gauge of the minimum load that we would require to reach an indentation, $b$ is linked to the loosed energy to create a novel surface per unit area, and $c$ is the power necessitated to create a lasting deformation of unit volume which can also be considered as hardness value that non-reliant to a load. Analogously to the PSR model, the determination of true hardness [23] is obtained with two ways for the MPSR model as $H_{PSR}{}' = \frac{b}{26.43}$, and $H_{PSR}{}'' = \frac{F-a-bd_0}{26.43d_0{}^2}$.

### 3.5 Elastic/Plastic Deformation (EPD) Model

Traditional indentation HT includes the measured size of a plastic impression remaining in the sample as a function of the indenter load. In microhardness tests, the indentation size is computed after eliminating the sharp indentation from the top of the sample that was an impression of residual surface. This impression includes some slowing of the unloading, which means that the unloading process arises flexibly. Owing to this impression, the indentation size would be somewhat reduced [24]. In this characteristic, the measured indentation size can be changed by a refined expression to compute true hardness [25].

$$H_{EP} = A\frac{F}{(d_0 + d_c)^2} \tag{11}$$

where $A$ is a constant that is depends on the indenter shape,$d_0$ is the variatio n in the indentation size, and $d_c$ credited to the elastic recovery. To study the numbers of nano indentation, the previous equation can be rewritten as

$$F^{1/2} = \beta^{1/2}d_0 + \beta^{1/2}d_c \tag{12}$$

where $\beta = H_{EP}/A$ is constant correlated to the true hardness. The plots of $F^{1/2}$ versus $d_c$ yields to $d_0$ and $\beta$ values.

### 3.6 Indentation-Induced Cracking (IIC) Model

In an endeavor to elucidate the inverse ISE, Li and Bradth [26] have believed that the applied indenter test load is balanced by the total resistance of the four-component sample at the point of maximum penetration throughout a loading half-cycle owing to: (i) frictional effect at the interface of sample/indenter, (ii) elastic deformation, (iii) plastic deformation, and (iv) sample fracturing. Conferring to Li and Bradth [26], indentation cracking participates to RISE, whereas elastic and frictional effects conduce to normal ISE. The PSR model proposed by Lee and Bradtht [22, 27] took into consideration the elastic and frictional effects. In indentation cracking case, the evident hardness is measured as [26]:

$$H_v = \varepsilon_1 K1\left(\frac{F}{d^2}\right) + K2\left(\frac{F^{1.66}}{d^3}\right) \tag{13}$$

Here, $d$ is the indentation mark diameter. $K1$ is associated to the geometry of indenter, $K2$ is dependent on the applied load. For a perfectly plastic material, $H_v = \varepsilon_1 K1\left(\frac{F}{d^2}\right)$, $\varepsilon_1 = 1$, and for a perfect brittle solid $K2\left(\frac{F^{1.66}}{d^3}\right) = 0$ while $\varepsilon_1 = 0$ [27]. $H_v = \varepsilon_1 K1\left(\frac{F}{d^2}\right) + K2\left(\frac{F^{1.66}}{d^3}\right)$ is applicable if there are no elastic recoveries occur after the elimination of load. For an ideal brittle material like superconductor materials, true hardness can be written as:

$$H_v = K\left(F^1.66/d^3\right)^m \tag{14}$$

Here $K$ and $m$ are constants that are non-reliant to both the load and the material adopted during the measurements. For m higher than 0.6, the ISE behavior is occurred whereas for the value of m less than 0.6 the RISE behavior is dominant.

From microhardness measurement, other important parameters can be extracted like fracture toughness ($K_{IC}$), elastic modulus ($E$), yield strength ($Y$) and by using the following expressions:

$$K_{IC} = \sqrt{2Ex}\ (\text{x, surface Energy})(\text{Pa.m}^{1/2}) \tag{15}$$

$$E = 81.8635 H_v\ (\text{GPa}) \tag{16}$$

$$Y = H_v/3(\text{GPa}). \tag{17}$$

# 4 Mechanical Nature of Alloy Superconductors

## *4.1 Niobium-Titanium Nb–Ti*

Since the discovery of superconductivity in 1911, the practical applications of superconductivity and the fabricating techniques of superconductors have been increasingly advanced over many decades. Niobium (Nb) is as an alloying element inserted to superalloys and melting steels in the form of Ni–Nb alloys or Fe–Nb. Nb-compounds ($Nb_3Ge$, $Nb_3Sn$, $Nb_3Ga$, and $Nb_3Al$), Nb-alloys or pure Nb, have applications that are more particular, are formed in tinier quantities and expensive. Pure niobium shows a superconducting state at extremely low temperatures. High purity superconducting Nb can be employed to produce superconducting accelerator cavities to hasten charged particles. The effective accelerators necessitate that the microstructure of Nb be altered to obtain excellent physical and mechanical characteristics [28]. Nb shall be malleable enough that it deforms according to the geometry of the resulting conceived cavity, and shall elaborate, throughout the plastic deformation, a smooth internal surface in the cavity. It has been revealed that the Nb microstructure has a great influence on the mechanical and physical properties of the characteristic's niobium [29]. A heterogeneous microstructure conduces to an uneven surface in the resulting cavity which may reduce the cavity efficiency.

In 2006, a group from USA reported the mechanical characteristics of high pure niobium sheets, which are exploited in the manufacture of the superconducting accelerator cavity [30]. Several tests have been adopted to evaluate the mechanical behaviors of high pure niobium sheets. TT was managed based on the standard ASTM E517 with the strain rate of $5 \times 10^{-3}\ s^{-1}$. TT samples were scratch in the sheet plane from five various directions of 0°, 22.5°, 45°, 67.5°, and 90°, as compared to the rolling direction., Three tensile samples were employed for each direction. To accurately estimate the transversal and longitudinal strains, the longitudinal and transverse extensometers were integrated on tensile samples. The engineering strain–stress plots showed that high pure Nb showed a mean elongation of about 50%. Also, the yield stress variations versus of the direction of rolling was plotted. The results showed that the yield stress is maximum in the 45° and achieved its minimum value in the 22.5° direction.

Although pure niobium shows a superconductivity phenomenon at low temperature, there exist several Nb compounds and Nb solid solutions (Nb–Zr, Nb–Ti,) that have improved superconducting characteristics [31]. Since 1960, the niobium-titanium (Nb–Ti) alloy has been the leading commercialized superconductor employed for magnet windings owing to its high critical current density, ductility, and strength [32]. Besides, Nb–Ti remains the low-priced superconductor for applications in the liquid He temperature area, since the starting materials and prices are much lesser compared to other superconductors. The principal applications of NbTi are in MRI, NMR, superconducting magnetic energy storage and particle accelerators. Because of its good ductility, Nb–Ti alloy can be warped into long wires.

In almost all commercialized Nb-Ti wires, usually with Ti contents ranging from 45 to 65 (wt.) %, show an exceptional arrangement of $T_c$, $H_c$ and $J_c$. Generally, high content of Ti rises the hardness of Nb–Ti filaments and can lead to sausage filaments and even the rupture of the filament [33, 34]. Since the diameter of the filament is typically less than 10 μm and even less than 1 μm, it needs that the primary composition of alloy be regular on the whole casting alloy. Hence, no Ti–rich zone, or unfused niobium are allowed in the primary Nb–Ti alloy. Z Guo et al. [35] have studied the mechanical characteristics of fine Nb-Ti filament with heat processing treatment. The authors calculated the hardness using Vickers hardness tester. They showed that the hardness upsurges when the strain of the wire rises, and cold work constantly increases the hardness of the filament. The initial of treatments rise the filaments hardness by 6% to 12%. This is attributed to the precipitates of titanium. The extra heat treatments reduce slightly the filament hardness (around 2–4%), where Nb-Ti cold work solidifies, although precipitation continues to increase. By means of tensile testing, Z. Guo et al. have measured the stress–strain curve of Nb–Ti fiber having a diameter of 67 μm down to 9 μm. Around 400 Nb–Ti fiber samples have ben measured. The result showed that the mechanical behavior of fibers of were affected by heat treatment. It was found that the strength of fiber diminishes by around 6 to 11% in the final heat treatment. The higher the heat treatment, the lower the strength of fiber was. The authors ascribed this effect to the precipitates of titanium that were produced with high temperature. Yet, when the size of the fiber is small due to the large effect of strain hardening, the impact of heat treatment become trivial. The authors have also determined the Yong's modulus (E) of 67 μm fiber. Their results showed that as the temperature increases, E increases accordingly. The authors ascribed this effect to the formation of titanium precipitates that results in high atomic percent of niobium of the matrix. In another study, He Liu et al. [36] have studied the mechanical behavior of Nb-Ti superconducting wires and evaluated its evolution with the wire size, geometry and volume ratio of the components and the influence of heat treatment at last obtaining wire sizes. To comprehend the mechanical characteristics of the Nb–Ti composite, mechanical assessments of the copper matrix, individual composite components, and Nb–Ti filament were carried out. The results showed that for the mono filamentary composite, copper matrix and Nb–Ti filament, can be utilized as the expectation of the ultimate tensile strength (UTS) of the composite. For the multi filamentary composite, the three components bring about the composites; a low strength, a high strength Nb–Ti fiber, high ductility bulk copper matrix and a medium strength (between bulk copper matrix and the Nb–Ti fiber) inter-filamentary copper matrix. Besides, Nb–Ti alloys are employed in superconducting cables, and orthodontic/orthopedic grafts [37, 38].

Generally, manufacture of Nb–Ti alloys begins with melting and ultimately re-melting in a vacuum arc re-melting (VAR) oven. An alternate processing stage is EBM (electron beam melting). EBM has significant benefits: this process improved hardness, ductility, and superconducting characteristics, and relatively low resulting amounts of interstitial elements (N, H, O, and C) can be formed [39]. Though, EBM has some disadvantages because of the hard monitoring of the chemical compositions

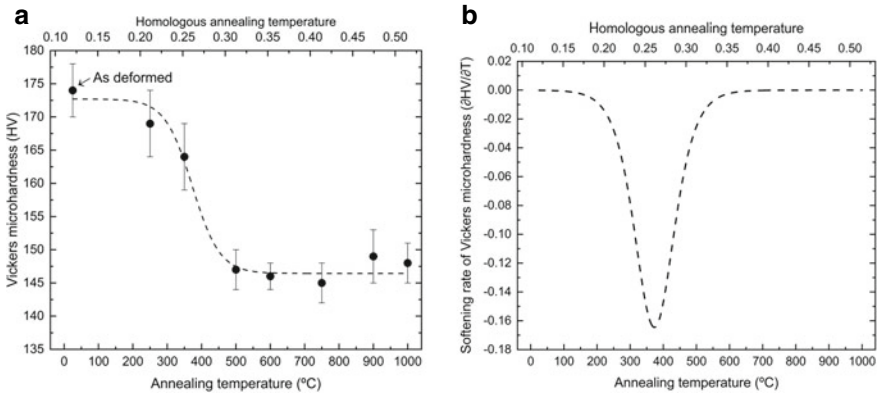


**Fig. 5** **a** $H_v$ measurements of specimens exposed to annealing cycles of 1 h. **b** softening rate of $H_v$ versus the homologous and annealing temperatures. Reproduced with permission from Ref. [39]

owing to the Ti evaporation under high vacuum during the melting and the accurate elements separation during solidification [39]. A probable following processing stage for the alloys of Nb-Ti is the plastic deformation of the cast alloys. Due to its high ductility and manufacturability, rods of these alloys with diameters of more than a few centimeters are plastically distorted onto micrometer filament to make superconducting cables [40]. Intermediate annealing cycles are frequently compulsory during mechanical treating, producing phase deposition, retrieval, and recrystallization, which may considerably alter the microstructure of warped alloys and their superconducting characteristics [41]. In a recent study, Andrei Marx Ferreira et al. [39] have examined the effect of recrystallization and recovery on texture and microstructure of a cold distorted Nb-50 (wt.) %Ti alloy superconducting. The measurements of Vickers microhardness were carried out with a load of 2 N.

Figure 5a displays the measurements of Vickers hardness versus the annealing temperatures and isotropic annealing. This figure showed a characteristic reduction as the temperatures are increased. The decrease is almost completed at 500 °C. The authors attribute this effect to recovery. The sigmoidal plot of $H_v$ data was regulated (Fig. 5b). The rate of the decrease was computed, and the maximum decrease rate happened at around 380 °C.

## *4.2 A-15 Niobium-Tin $Nb_3Sn$*

The niobium-tin $Nb_3Sn$ is another important commercialized alloy with A-15 crystallographic structure. Getting $Nb_3Sn$ superconductor that meet very stringent necessities regarding their properties and, in particular, their current transport capacity is one of the topical problems in creating magnetic systems for up-to-date elementary particle accelerators, like High Luminosity-Large Hadron Collider (HL-LHC) [42].

The upgrade of the LHC [43] at CERN involves replacing, at certain points, the main Nb–Ti-based dipole by two 11 T-based $Nb_3Sn$ dipoles [44]. Under the HL-LHC project, there are $Nb_3Sn$ coils impregnated with epoxy resin at the center of the $11_T$ magnet and other high-field magnets. In this status, it is verified that the $Nb_3Sn$ Rutherford cable that makes the coil, displays an irreversible deterioration in operation when exposed to too much loading [45, 46]. It is so compulsory to examine the mechanical features of the coils, to monitor and improve the stresses generated during assemblage and operation steps, involving the cooling period. Owing to its brittleness, $Nb_3Sn$ cannot be distorted directly into wires as performed for Nb–Ti alloys.

Numerous kinds of procedures can be adopted for wires manufacture involving bronze process (began with the bars of Nb alloy enveloped with ductile Cu-Sn bronze and then amassed within another Cu-Sn tube to get a multi-filament structure), Sn internal process (began by locating the core of Sn in the middle of the Nb strands implanted in the copper matrix), and the PIT process (began with by filling Nb–Sn powders rich in Sn such as $NbSn_2$, and $Nb_6Sn_5$ into niobium tubes). Through cold wire heat treatment, the $Nb_3Sn$ phase can be gotten by the reaction between Nb and Sn. The main to improving $Nb_3Sn$ wires is to enhance their trapping ability. Since the pinning of grain boundaries in $Nb_3Sn$ is neither as effective nor intense as α-Ti pinning in the Nb–Ti alloy, fine-tuning of grain of and the artificial pinning cores are operative in the flux trapping. Owing to the increasing complexity of wire fabrication, the $Nb_3Sn$ superconducting wires commercialization was achieved after 1970, with a somewhat higher cost than that of Nb–Ti superconductors. Since that time, $Nb_3Sn$ has been widely studied by numerous researchers worldwide for practical applications. Magnets high-field $Nb_3Sn$ for the next generation of hadron colliders are recognized to have an elongated and restricted drill by 90% of the short specimen limit at best, implying that the current of conductor is at 60% or lower than its critical value. Monolithic finite element models are usually exploited for a complicated system that contains wedges, coils, yokes, shafts, fillers, bars, wrenches, shoes, casing, etc.

Measurements of mechanical properties allow for a well comprehension of strain and stress distributions. This is very necessary for the functioning of $Nb_3Sn$ since modern high-critical current wires are mostly sensitive to strain. Emanuela Barzi et al. [47] measured the mechanical properties of $Nb_3Sn$ cables, coils, and strands. For this purpose, tensile testing of cold-worked copper, unreacted Nb-Sn, and annealed copper wires were gauged at room temperature using an Instron machine. More than 15 specimens tested, the final average stress of the former was 630 MPa ± 5%, and above 11 tested samples, the Young's modulus of the latter was found to be 53 MPa ± 10%. Jose Luis Rudeiros Fernandez et al. [45] measured experimentally the mechanical properties of $Nb_3Sn$ Coils. Their findings demonstrated that the compression behavior of the entire conductor block, and the structure of the coil composite is nonlinear in the analyzed zone, while displaying high levels of nonlinear stress stiffness, even from moderately low stress levels. Furthermore, lasting plastic deformation was also detected from minimum levels of mid-level stress. Given that $Nb_3Sn$ is brittle, and its superconducting characteristics are sensitive to the stress,

a group from CERN, Austria, and Germany aimed to study the irreversible degradation of critical current with the mechanical prestressing, which is exerted to the interacting and saturated $Nb_3Sn$ coils for accelerator magnets at room temperature [46]. The reactive and impregnated cables of $Nb_3Sn$ were subjected to rising tangential compressive stress up to an extreme stress level of 200 MPa at room temperature. After each cycle of compression, the critical current of the cable samples was marked at 4.3 K at the FRESCA Cable Test Station. No serious degradation of the current was observed up to 150 MPa, tracked by a degradation of less than 4% after a nominal stress of 175 MPa. A lasting remarkable decline of the critical current arisen after an application of pressure of 200 MPa.

## *4.3 Niobium Aluminide ($Nb_3Al$)*

The advance of A15 high-current superconducting superconductors capable of carrying current in extremely high magnetic fields is known as an allowing technology for the design of second-generation NMR magnets functioning at frequencies above 1 GHz. The ternary metal alloy $Nb_3Al$ has been known as an exceptional source of future multi filamentary superconductors able of operating at magnetic fields well above 25 T and in severe irradiation and mechanical conditions [48]. $NbAl_3$ is stable up to elevated temperatures exceeding 1000 °C. Magnetic fields above 40 T have already been measured without defeat of superconductivity for some $Nb_3Al$ compounds [48]. If this type of inter-metallic material can be established in the form of wire, it will lead to a new invention of commercialized high-magnetic field magnets, like those needed for NMR spectrometers to operate in the 1000 MHz. $Nb_3Al$ are interesting owing to their high elasticity modulus, high melting point, outstanding oxidation resistance, and low density. Moreover, $Nb_3Al$ can be an alternate to $Nb_3Sn$ for high-magnetic field applications. However, it is extremely hard to exploit $Nb_3Al$ alloys as single-phase for applications due to the extreme brittleness at room temperature. The single-phase $Nb_3Al$ alloy exhibits a fracture toughness, $K_{IC}$ with a value as small of 1.1 MPa $m^{1/2}$[49]. Therefore, inclusion of a tougher phase solid solution like Nb ($Nb_{SS}$) can be one operative method to improving the $K_{IC}$ at room temperatures, even though it will lead to a reduction in the strength at higher temperatures. Accordingly, Nb-based in situ compounds like Nb/$Nb_3Al$ [50] have been established.

The development of Nb/$Nb_3Al$ as possible high-temperature structural material, in which solid metal particles are incorporated into Nb solid solution and there are no interfacial interactions due to interfacial stability even at extremely high temperatures. But, both the oxidation and fracture characteristics of these alloys are insufficient for high-temperature structural applications [51]. Hence, further improvement is required by alloying additives in Nb-based in situ composites. L.M. Peng have synthesized niobium aluminide-based composites and studied their mechanical behaviors at ambient temperature [52]. The mean value of flexural strength is 356 and 368 MPa for Al40Nb60 (at.%)–$TiO_2$20C8 (wt.%) and Al30Nb70 (at.%)–$Al_2O_3$10TiC10 (wt.%)

based composites, respectively. Also, these composites displayed a corresponding value of $K_{IC}$ of 5.3 and 5.6 MPa $m^{1/2}$. From these results, the authors concluded that both the in-situ created and externally added fine $Al_2O_3$ and TiC particles are efficient in improving both the fracture toughness and strength of the $Nb_3Al$ via interactions among the microstructure and crack tip. This improving effect could be ascribed to the protecting effect throughout crack spread through crack deflection and crack bridging under compressive stress, induced by the mismatch of lattice coefficients and thermal expansion coefficients between the second phase particles and the matrix.

## 5 Mechanical Properties of High $T_c$ Cuprate Superconductors

High $T_c$ superconductors (HTS) possess high $T_c$ above the $LN_2$ temperature (77 K). Owing to the very rich nitrogen abundance, the price of cooling with liquid nitrogen ($LN_2$) is extremely inferior than liquid helium (LHe), which renders it achievable for large-scale industrial applications. The rare earth-based cuprates (REBCO) and bismuth-based cuprates (BSCCO) are among the well-known HTS. Although the $T_c$ of the REBCO and BSCCO is much superior than that of $Nb_3Sn$ and Nb–Ti alloys, they are very hard to treat with tapes and wires due to their ceramic fragility. HTS display great critical current density and good trapped magnetic field at cryogenic temperature [53–58]. Yet, practicable applications of these HTS are frequently limited. The weak mechanical characteristics of HTS stand in the avenue of a large range of real applications. This is due to the lack of slip planes in the oxide materials, which kills the ductility of HTS and increases their brittleness. During the discovery of HTS, great interest has been paid to the improvement of the mechanical behavior of these materials to expand their practical implementations. One of the most interesting characteristics to be enhanced for engineering applications of these materials. are the micro hardness, elastic modulus, creep behavior etc.

### *5.1 BSCCO Superconductor*

Bismuth-based HTS class is epitomized by the common formula $Bi_2Sr_2Ca_{x-1}Cu_xO_{2x+4}$ (x = 1, 2, and 3, corresponding to Bi-2201, Bi-2212, and Bi-2223 phases, respectively). The former two phases are recognized to have some significant characteristics for the research development, and applications in industry and technology. Among these three phases, Bi-2223 looks to be the most talented candidate for power transmission cables application at the temperature of $LN_2$ owing to its high critical temperature, $T_c$ (110 K). Nevertheless, there are some main restrictions for the practicable applications of Bi-2223, which are

linked to their ceramic nature: they are relatively brittle, highly anisotropic, exhibits small critical current density ($J_c$) at elevated temperatures and hard to form as a single-phase. The practical applications will necessitate, particularly, the assessment of mechanical characteristics.

The strength and plasticity of BSCCO can be rigorously influenced by numerous defects: twins, micro-cracks, dislocations, pores, and ordering defects. Consequently, enhancement of the mechanical features of BSCCO is a main research purpose. It is probable to restrain the intrinsic brittleness of these superconductors and disclose an apparent plastic flux with dislocation creation by distortion at high temperature, and at ambient temperature by applying a hydrostatic pressure, or by doping [59, 60]. S.M. Khalil showed an enhancement of the mechanical behavior of BSCCO by doping it with lead [61]. Microhardness investigations on chosen smooth surfaces of the samples studied were performed at room temperature by exposing the surface of sample to standing indentation tests. The load was ranging between 0.15 and 0.98 N. For all indentations, the duration of indentation was 15 s. Indentations were performed at various positions of the surface's sample so that the distance linked two indentations was greater than 3 times the diagonal of the inden mark to prevent the effects of surface because of neighboring indentations. For each sample, many attempts of indentation with each load were performed and then the mean value was calculated. The hardness $H_v$ is around to 1.14 MPa for a load of 0.15. The hardness decreases as the load decreases. The authors attribute this behavior to many reasons: (i) at greater indentation loads, the $H_v$ showed low values, this can be owing to the existence of weak links in the ceramics; (ii) at low indentation loads, the $H_v$ presented high values, this is credited to the fact that the values of measured hardness were more suggestive of the mono-crystal case with the absence of overlap from the grain boundaries. Interestingly, the hardness showed an increase with increasing the content of Pb in the BSCCO and the maximum value of 3.25 MPa was obtained for $x = 0.3$. The Young's modulus as well as the yield strength increase with Pb addition. M. Anas studied the mechanical properties of BSCCO added with $PbF_2$. The results showed that a 0.1% $PbF_2$ added to BSCCO phase enhance its mechanical property. The data of s micro hardness were analyzed by various approaches and a good concurrence with PSR model was demonstrated [62].

BSCCO wires can be implemented in power electric devices including NMR, MRI in high magnetic field. During magnet fabrication, a complex stress/strain is engendered during pulling and twisting, and during its activation, a great electromagnetic force is exerted to the superconducting wires due to their high $J_c$. Hence, it is interesting to have comprehensive awareness of mechanical and electromagnetic features of superconducting wires. Bi-2223 tapes have been effectively commercialized using monitored overpressure technology. To be exploited in high-magnetic field applications, enhancements in their current transport capacity are still required under significant stress/strain conditions as well as better mechanical characteristics. The tapes have been strengthened by means of sheet metal lamination including stainless steel, copper alloy, and nickel alloy, which improves both critical current stress tolerance and yield strength [63]. To properly comprehend these enhancements, mechanical

properties and the effect of the local strain applied on the BSCCO filaments themselves are required. For instance, Kozo Osamura et al. [64] studied the mechanical property of Bi-2223 wire laminated by stainless steel. It is found a linear decrease of $J_c$ in BSCCO tapes in a small zone of tensile stress and a reversible return of $J_c$ upon stress reduction. On increasing the tensile stress beyond the typical value, $J_c$ dropped quickly because of the brittle breakage of the BSCCO filament. A Godeke et al. [65] have conducted systematic research of the appropriateness of the high strength DI-BSCCO type HT-NX (this type has been declared in 2014 by SEI which is covered with a high-strength nickel alloy) for high-field solenoid applications. The authors found strain limits of 0.92% and higher, flexibly calculated at the exterior border of the conductor. Thus, in coils subjected to single bending during twisting with loop stress, a strain limit of 0.92% appears to be relevant, which renders DI-BSCCO type HT-NX very appropriate for the input coils of high field solenoid magnets. Bi-2212, another correlated Bi-based HTS, can be made as a multi-filament round wire by using powder-in-tube method, nonetheless a high pressure (up to 100 bar) is needed during high temperature oxygen handling to attain highest critical currents. Bi-2212 is produced in an isotropic, circular, multi-filament form that can be coiled or bonded into random geometries including Rutherford cables. Bi-2212 will also enable high-field magnets that exceed the proton NMR current limit of 1 GHz (23.5 T) for Nb3Sn technology.

Tremendous progress has been made in its development for exploitation in high-field magnets since the demonstration of a multi-filament circular wire Bi-2212 by Oxford Instruments. The Chinese Fusion Engineering Test Reactor is a novel tokamak design whose magnet scheme contains a central solenoid (CS), toroidal field (TF), and poloidal field coils (PF) consisting of a cable-in-channel conductor (CICC). Bi-2212 HTS is a promising magnetic material for CICC because it displays good superconducting carrying capacity at low temperature of 4.2 K under magnetic field, particularly for high-pressure heat-treatment. Nevertheless, the Bi-2212 phase is a stress-sensitive ceramic. So, the mechanical property is of great significance for its application. In this context, Zhe-Hua Mao et al. [66] studied the mechanical property of Bi-2212 round wire using standard and high-pressure heat treatments at 300, 77 and 4.2 K. The authors found that the wires treated at 50 atm high-pressure heat treatment exhibited upper mechanical strength than that treated under 1 atm standard pressure. Hence, high-pressure heat-treating Bi-2212 could be ideal choice to enhance the performance and mechanical strength of wires, rendering them promising for conductor design and upcoming manufacture.

## *5.2 REBCO Superconductor*

Contrasted to BSCCO superconductors, REBCO (RE: rare earth elements) exhibits lower anisotropy and higher $J_c$ in the presence of field at 77 K. Yet, the uniaxial aligned grain structure (c-axis) attained in BSCCO wires by melting or rolling induced texture is insufficient for REBCO, so it is necessary to achieve high $J_c$ and a bi-axial grain

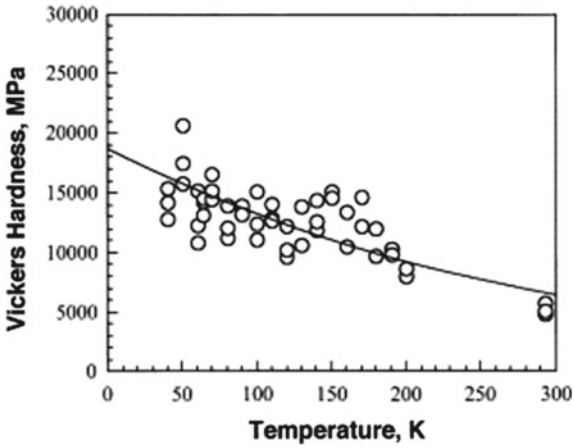


**Fig. 6** Temperature dependency of Vickers hardness for bulk YBCO. Reproduced with permission from Ref. [67]

texture. REBCO superconductors fabricated by the usual sintering method are recognized to be mechanically extremely brittle and of concern in their practicable applications. The cause for the fragility is principally the existence of pores in the ceramics with a restricted plastic deformation extent. During the past years, the mechanical characteristics of YBCO have been examined at cryogenic temperature called work temperature ($T_w$) or at room temperatures. The most chief characteristics evaluated have been the elastic modulus, E, the hardness, H, the toughness fracture, $K_{IC}$, and the yield stress. These parameters can be measured by different techniques. Yoshino et al. [67] measured the Vickers hardness $H_v$ of bulk YBCO at temperatures ranging from 40 to 290 K by means of the cryocooled-type Vickers hardness tester. $H_v$ was found to be $5.2 \pm 500$ GPa at room temperature. $H_v$ was boosted by about 3.5 times on decreasing the temperature. High hardness dispersion was observed at cryogenic temperatures (Fig. 6). Generally, hardness bulk YBCO are in the range of 5–8 GPa at room temperature [67, 68] and increases with decreasing the temperature [69].

Numerous efforts have already been done to surpass this drawback. For instance, silver-coated REBCO-sealed ceramic powders are pulled into a wire or a mixture of superconductor ceramic and gold or silver-metal powders sintered to produce composite materials. Matsumuro et al. [70] treated the mechanical characteristics of YBCO/Ag composites made at high pressures of 2.0 and 5.4 GPa. The YBCO/Ag composites were made by mixing Ag and YBCO powders in different volume ratios (0 to 100%). The mechanical characteristics typified by the maximum strain and the compressive strength were found to be improved 2 to 3 times, compared to the pure YBCO made under the normal pressure of lower than 1 GPa. C. E. Foerster et al. [71] investigated the mechanical characteristics of silver-doped top-seeded melt-grown YBCO pellets. The different contents of $Ag_2O$ were in the range of 0.0–15 wt.%. Elastic modulus and hardness were gotten by fracture toughness and instrumented indentation by traditional Vickers indentation. The supreme values of elastic modulus and hardness were attained for a content of 5 wt.% $Ag_2O$. The hardness was around 9000 MPa for 5 wt.% $Ag_2O$ content whereas it was about 8000 MPa for virgin YBCO.

With further increasing silver concentrations, the hardness reduced to 7000 MPa. The elastic modulus was also increased from 180,000 MPa for pure sample to reach its maximum value of 220,000 MPa for 5 wt.% $Ag_2O$ concentration. The $Ag_2O$ doping also improved the indentation $K_{IC}$ from 1.43 MPa $m^{1/2}$ for virgin sample to 1.6 MPa $m^{1/2}$ for sample mixed with 10 wt. % of $Ag_2O$. Kölemen et al. [72] studied the impact of 1.0 wt.% ZnO on the mechanical behaviors of YBCO bulk. For pure sample, the hardness at ambient temperature was equal to 517 MPa and increasing with decreasing the temperature. For example, an enhancement by a factor ~3.5 at T = 40 K. Great scattering was found at cryogenic temperatures. For YBCO added with 1.0 wt% ZnO sample, $H_v$ at ambient temperature was equal to 1075 MPa and increased at 40 K to 2316 MPa.

For numerous types of materials, apparent microhardness is dependent on applied load. Generally, hardness shows an almost decrease in parabolic behavior when increasing the load applied and tends at high applied loads to a plateau with nearly constant hardness values. According to U. Kölemen et al.' study, the hardness rises as ZnO content increases. The authors attribute this effect to ZnO addition that can rise the mechanical strength of ceramics by precipitation hardening mechanisms and solute solution. On the other hand, YBCO conductors can withstand high tensile stresses up to 0.7 GPa [5–7]. Hence, YBCO-coated tapes are suitable for NMR, accelerators and generators. For mechanical strengthening in defiance of giant Lorentz forces under elevated magnetic field, impregnating YBCO coils with epoxy resins are frequently employed. Nevertheless, epoxy resins exhibit dissimilar thermal expansion coefficients compared to YBCO HTS tapes. Naturally, at 77 K, epoxy resin dwindles around seven times more than metals. Over the cooling process, the shrinkage of the epoxy resin not only engenders tangential stress on the YBCO tape's surface, but also produces cleavage stress at the YBCO tape border. Due to the laminating structure, YBCO-coated tapes cannot withstand tangential stress beyond 10 MPa [73] and cleavage stress beyond 0.5 MPa [74].

Many researches indicated that thermal expansion mismatch led to conductor damage and critical current degradation in epoxy-impregnated YBCO HTS coils. Numerous methods have been anticipated to resolve the problematic, such as the usage of polyester thermal shrink tube (PTST) [75], no-insulation (NI) technique [76], paraffin impregnation [77]. Generally, the mechanical strength of paraffin is relatively low. At low temperatures, paraffin is brittle so it is not easy to offer the entire mechanical stability for the magnet in an elevated magnetic field. The PTST method although it gives good results under the application of high field magnets [75], it is complex which may constrain its applications. In NI technique, no critical current degradation was observed. Until now, an YBCO HTS magnet with no-insulation technique has effectively attained 26.4 T at low temperature of 4.2 K. But, if the magnetic field exceeds 30 T, the NI technique might not deliver sufficient mechanical strength for the YBCO magnets. Tomita et al. [78] showed an enhanced mechanical characteristic of YBCO bulk superconductor prepared with carbon fiber fabrics. Using a tensile tester, the authors measured the tensile strength of YBCO bulk. The tensile strength was significantly improved by coiling the bulk YBCO with a carbon fiber fabric before impregnating with resin. The mechanical characteristics of

YBCO large grains were examined by strain measures. The electromagnetic pressure was executed on the specimens at 65 K by decreasing the exterior field from 7 to 0 T. The bulk sample was cracked in the absence of resin throughout the field decrease process with a supreme stress of 150 MPa. However, the highest pressure was merely 40 MPa for the resin-impregnated specimen coated with carbon fiber fabrics. These findings showed that covering the bulk YBCO with carbon fiber fabrics could influence positively in steadying the mechanical characteristic and improving the tensile strength. In another study, Guangda Wang et al. [79] proposed to exploit, for the first time, ice to impregnate YBCO HTS coils for insulation and mechanical strength. This new method based on ice impregnated coil allowed to get superior mechanical strength than that of the paraffin impregnated coil. This is helpful for the appliance of YBCO HTS coils in the high magnetic field. In addition, this method is cost-effective and easy to process. Also, the YBCO tapes can be repetitively employed after impregnation. As a perspective for this study, the authors have proposed to quantify the insulation and mechanical strength of the ice impregnated YBCO and to further explain the avoidance of the critical current degradation in future studies.

Additionally, carbon-based compounds played a leading role in enhancing the mechanical features of REBCO due to their extraordinary hardness caused by SP2 bonds between the individually arranged carbon atoms. For example, a study performed by Anas et al. [80] showed that the microhardness Hv was improved by low addition of single and multi-walled carbon nanotubes into REBCO (RE = Gd). The microhardness measurements were performed at room temperature in air using a IN-412A Vickers microhardness tester. The load applied changes between 0.5 to 10 N for a loading duration of 40 s. For each load, the mean value of $H_v$ was computed by considering five readings at various positions on the specimen's surface. The Vickers microhardness $H_v$, elastic modulus E, the yield strength Y, and the fracture toughness $K_{IC}$ were determined and showed an enhancement with small addition of CNTs. $H_v$ drops quickly when the applied load increases then it inclines to be saturated. This is due to ISE effect. Besides, this effect is associated with the indenter penetration depth; for low loads, the indenter enters only the surface layers, accordingly the surface effect is dominant. Though, when the penetration depth rises, the effect of internal layers is overlooked, for this reason, the value of $H_v$ is unchanged for high load was occurred. The authors also demonstrated that Hv boosts when CNTs addition increases up to 0.08 wt.%. This enhancement is credited to the diminution of the degree of porosity and the improvement in inter-connectivity. REBCO (RE = Y) HTS can be combined with polymer matrix to fabricate composite materials with good mechanical characteristics, flexibility, and greater processing capacity. They can be simply modeled into several suitable forms by multipurpose polymer processing methods like extrusion, injection molding and, compression.

It is difficult to achieve an exceptional combination of good insulating and mechanical traits in a single-component material. Pure polymers are simple to treat as mechanically strong components but commonly suffer from a minimal dielectric constant [81]. Additionally, ceramics are fragile and need an elevated temperature [82] which is frequently incompatible with existing with integrator technologies. The perfect solution would be incorporated adequate polymer to the mechanically

robust materials to form polymer/ceramic composites that may meet the anticipated characteristics of the components [83]. Rosalin Abraham et al. [84] have studied the mechanical behavior of YBCO/polystyrene composites. Tensile properties were examined using ASTM D638. The Young's modulus of the composites increases on augmenting the filler YBCO concentration. However, tensile strength and elongation at break of the composites diminish with filler addition.Similarly, Kupchishin and co-workers [85] reported the impact of YBCO filler on mechanical characteristics of composites-based polyimide. Mechanical measurements were done on the tensile tester. Their findings showed that the introduction of YBCO filler into the polyimide induces an important change in strength and plastic characteristics of polymer matrix. Recent work performed in 2019 by Tomas Hlasek et al. [86] reported the mechanical behavior of single-domain YBCO bulk superconductor treated with artificial holes (Ahs). The samples were fabricated by a traditional top-seeded melt growth method. Ahs were included to the green sample before the process of heat treatment using a detailed "toothed" mold. Mechanical characteristics including Vickers hardness, tensile strength, compressive strength, and modulus of elasticity were measured. Their results showed that the hardness is somewhat higher for the sample holding Ahs. At 77 K, the hardness was increased from around 5.29 GPa for standard pellet to about 6.17GPa for pellets wit Ahs. The elastic modulus of the YBCO with Ahs was enhanced by more than 45% at temperatures of 77 and 295 K. At room temperature, the ultimate tensile strength was also enhanced from 360 to 460 GPa for YBCO with Ahs. The results showed that filling bulk YBCO with holes is potential for improving the mechanical characteristics. Such method will further allow the thermal conductivity to be regulated and enhance the stability and applications range of the material, particularly in pulsed field magnetization.

The growth success rate of single-grain superconductors YBCO bulk, which are typically useful for trapping field magnets, by melt-processing methods is frequently relatively low. To guarantee that RE elements consumed in these systems are not lost, and to recover the production economics, an efficient method of recycling these "non succeeded" materials is indispensable to the prolonged-term sustainability of the bulk process. This has encouraged scientists to expand new methods to recycle these failed materials in moderately large numbers. Top seed melt growth is the commonly used method for preparation single-grain superconductors YBCO bulk. A substitute approach to TSMG is the TSIG (top-seeded infiltration and growth) process [87]. In this context and based on this idea, Devendra K. Namburi et al. [88] studied the mechanical characteristics via recycling YBCO superconductor. The mechanical measurements were performed by using nano-indentation technique to determine the elastic modulus ($E$) and hardness ($H$), 3 points bend test for the flexural strength, and Brazilian tests for tensile strength determination [88]. The hardness measurements showed that the YBCO-211 phase (non-superconductor) is harder (with elevated elastic modulus) than the superconductor YBCO-123. Besides, both the YBCO-211 and YBCO-123 phases are stiffer and harder than the $BaCeO_3$. More importantly, the prime grown samples prepared through the TSMG method are considerably stiffer and harder than the recycled samples. The authors correlated this effect to the

distinctions in distribution and the dimension of the microstructural phases (specifically YBCO-211 and YBCO-123). During the recycling process, more stresses in the YBCO-123 matrix can be generated owing to the mismatch in thermal expansion of the YBCO-123 and YBCO-211 phases. This would diminish hardness (and ultimately elastic modulus) of the recycled samples comparative to the initial produced samples. However, the flexural strength showed an increase from ∼50 MPa for the initial produced samples to ∼75 MPa for recycled samples. In addition, the maximum tensile strength is around 20.2 MPa for the recycled YBCO sample, which somewhat higher than obtained in the initial produced YBCO sample (∼19.1 MPa). All these results obtained indicated that the recycled bulk YBCO samples have important prospects for exploitation in industrial applications where the mechanical strength of the superconductor is a key concern and that the recycled samples may provide satisfactorily better superconducting traits.

## 6 Mechanical Properties of Non-cuprate High-$T_c$ Superconductors

### *6.1 Diboride of Magnesium $MgB_2$*

$MgB_2$ is an intermetallic material with a moderately high-Tc of ~40 K [89], which produces an innovative $T_c$ record in the metallic-type systems. Dissimilar from the HTS, $MgB_2$ exhibits benefits of rather simple crystal structure and chemical composition, great coherence length, low anisotropy, and cost-effective of raw materials. These benefits render it a talented candidate for small or mediocre magnetic field applications in the 20–30 K temperature interval. Owing to its brittle character, it is compulsory for $MgB_2$ to exhibit good mechanical behavior to resist the Lorentz force engendered by the magnetic field. The preparation method, doping effect can affect the mechanical behavior of $MgB_2$. Sintering processes under the high pressure, including spark plasma sintering SPS, the Reactive Liquid Mg Infiltration (RLMI) and hot isostatic pressing HIP, are operative in enhancing the packing ratio of bulk $MgB_2$ superconductor [90, 91]. Akira Murakam et al. [91] reported the mechanical characteristics of $MgB_2$ prepared by SPS at different temperatures of 950, 1000, and 1100 °C using bending tests. Strain–stress behaviors are nearly linear till the fracture. This linearity is usually observed for brittle materials. The Young's modulus and bending strength (stress at fracture) were enhanced by the rise of the SPS temperature. G. Giunchi et al. have adopted RLMI method for the synthesis of bulk $MgB_2$ and have studied their mechanical characteristics [92]. RLMI led to dense $MgB_2$ samples. The $H_v$ measurements were carried out in micro indenter tester by using a load of 1.961 N. The authors have measured $H_v$ in different regions of the samples. The results showed that $H_V$ is different from on region to another. The average $H_v$ value in inter-grain region is 1.9 GPa, lower than obtained in the large grains where the mean Hv value is 35 GPa. The authors ascribed this result to the existence of

impurity ($Mg_2B_{25}$) within the large grains. $Mg_2B_{25}$ is well known with its great hardness. In addition, the doping effect greatly affects the mechanical behavior of bulk $MgB_2$. Deeper information on this effect were discussed in REFs [93–96].

The extensive advance $MgB_2$ in wires form is aimed at wide range implementation of superconductors beyond what is reasonably feasible with low-temperature superconductors, operating at the temperature of LHe. This wire type may attain industrial performance levels for multi-applications. To determine the necessitated wire characteristics and validate the potential, works on different applications is required. $MgB_2$ conductors at CERN are exploited for the current connections to the LHC. Concentrating on the conductor $MgB_2$, there are many future applications, specifically in the mediocre magnetic field of 0.5–4 T range. Including these are induction heaters, high current cables, coils for MRI devices, engines and generators. $MgB_2$-based engines and generators are the basis for impulsion of ships, wind turbines (WT) and electric aircraft. Superconducting WT generators are driven by the relatively low size and weight that can be achieved when the magnetic field in the air gap is increased over 1 T [97], which is the maximum for long-lasting magnet-based generators. The central technology is the superconducting field coil of the rotor.

To evaluate technology and offer a wide range of engineering fabrication, various winding and wire methods must be evaluated and tested to get reliable coils at a depressed price. Practically, $MgB_2$ wire commonly requires a diffusion barrier averting the probable reaction that can occur between superconducting filaments within a good conductive metallic sheath. PIT method is extensively employed for fabrication of $MgB_2$ tapes and wires. In PIT process, the external sheath material (like Cu, Fe, stainless steel (SS)) plays a leading role in the densification of powder influencing the final the superconducting property especially Jc value [98]. In addition, the external sheath influences the tolerance to mechanical stresses [99]. Shielding barriers are frequently created of inert metals (like Ta, Ti or Nb) to minimalize or prevent any reaction between the outer sheet and Mg. Furthermore, using diffusion barrier renders the superconductor composite more complex and pricier, and reduces the load factor of the superconducting phase of the wire. Groove rolling, drawing, or biaxial deformation rolling processes are employed for $MgB_2$ wires with better performance [98]. An external sheath mechanically robust is particularly imperative for only drawing-deformed wires if a high density, and even filament structure is required [98]. I Husek et al. studied the mechanical behavior of multi-core $MgB_2$/Ti/Cu/SS wire treated at 500–850 °C [100]. The heat treatment has an impact on the mechanical behaviors of the prepared multi-core wire. A constant increase of hardness of filament with heat-treatment temperature was obtained. The hardness of the Ti barrier and Cu steadiness are unaffected for temperature annealing ranging between 500 and 650 °C. The $H_V$ of the SS sheath annealed at 500 °C–550 °C is greater than that obtained for as-drawn wire ($H_V = 560$ MPa) owing to probable transformation. Softening of the SS jacket contributed to annealing at temperatures exceeding 650 °C and the external jacket was less stiff than $MgB_2$ filaments after annealing beyond 700 °C. The authors were also calculated the plasticity (ε) and the mechanical strength of as-drawn and annealed wire at 600 and 800 °C. Their results showed that the strength was equal to 1200 MPa for the as-drawn wire, such a value

is extremely high and its plasticity relatively low (ε lower than 5%). The authors attribute this effect to high cold deformation of the SS sheath. A reduction by 24% in the strength of the wire and an almost variation in the plasticity was occurred when heat treating the wire at 600 °C. With further increase the heat treatment (800 °C), the strength was reduced by 57% and the plasticity was increased more than twofold owing to the changes of component and interface reactions.

On the other hand, many researchers have focused their works, in last decade, on $MgB_2$ thin films since they can be used effectively in manufacturing of numerous superconducting devices as Josephson Junctions, tunnel junctions, and field sensors. These devices are usually reserved at 4.2 K during working, and heated up when not in operation. Permanent thermal cycling generates stresses on the thin films. Correct knowledge of these stresses and potential failure modes requires the mechanical characteristics of $MgB_2$ thin films. In 2015, Ozmetin's group [101] reported the mechanical behavior of $MgB_2$ thin films by means of nano indentation. At an applied indentation load of 150 μN, the nano hardness is about 12.8 GPa. The values of nano hardness decrease with increasing the applied indentation load and become constant for high applied indentation load. This effect is due to ISE effect. To further explain the ISE effect, Ozmetin et al. used the PSR model for analyzing the experimental results. Reduced elastic modulus and nano hardness values were found to be equal to 178.13 GPa, and 11.72 GPa, respectively [101].

## *6.2 Iron-Based Superconductors (IBSc)*

The discovery of superconductivity phenomenon in IBSc in 2008 [102] has endorsed a great interest in the applied research on superconducting materials. These materials belong to the second family HTSc after the cuprates. They exhibit high critical fields and low electromagnetic anisotropy. Among the most important ISc materials are 122 type. The unique properties of 122 type IBSc render them highly talented candidates for high-field applications, which require high-functioning and cost-effective tape and wire conductors with great current transport ability to produce giant magnetic fields, satisfactory mechanical strength to resist the thermal stress and electromagnetic during work, and superconducting filaments in metal matrix for shielding against flow jumps and thermal cooling.

The possibility of producing 122-type IBSc tapes and wires with high-strength metals like Monel alloy Fe, and Cu renders them interesting for high-field purposes. More significantly, they can be made by an easy and effective price PIT method, which is favorable to mass manufacture. In term of covering materials, Ag is frequently used as an inert wall between the metallic sheath and the superconductor in the fabrication of the IBS type 122 multifilaments. For instance, Yao et al. [103] fabricated high strength seven-filamentary Sr122/Ag/Monel tapes, demonstrating practically no Jc reduction under a compressive strain of 0.6% [10]. Xu Guangxian et al. [104] suggested a rolling method–bi-directional rolling for 7-filament 122 tape. The impact

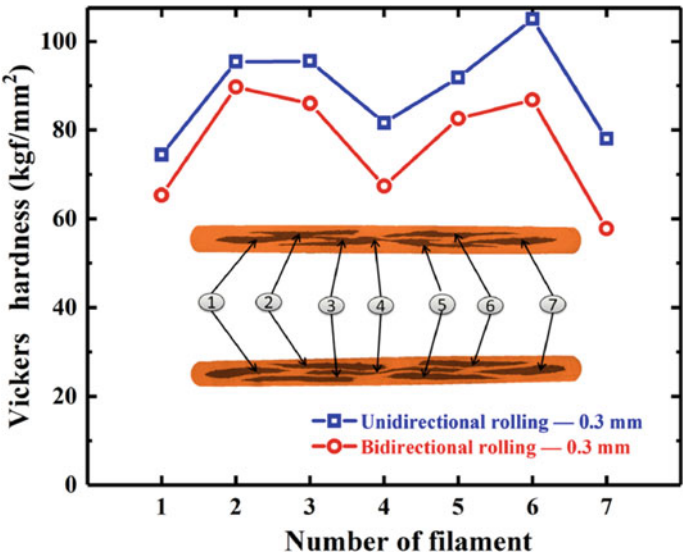


**Fig. 7** $H_v$ measurement of uni-directional and bi-directional rolled tapes for 0.3 mm for the superconducting filaments. Reproduced with permission from Ref. [104]

of rolling direction on the Vickers micro-hardness of 7-filament 122 tapes was examined. Vickers micro-hardness was performed by a transverse cross-sectional micro hardness tester with 50 g load and duration of 10 s. The hardness of uni-directional rolled specimen is greater than that of the bi-directional rolled tape at the respective position of each filament, which indicates that the filament density is further improved by uni-directional rolling than by the bi-directional rolling (Fig. 7). For example, for a number of filaments of 4, $H_v$ are about 0.88 and 0.60 GPa for uni- and bi- directional rolling, respectively. Since the direction of the force of the superconducting filament still steady for each track in the uni-directional rolling, the superconducting filament permanently distorts in the identical direction, which leads to an increase in the density of the core. Additionally, the central layer of superconducting filaments, whose positions are far from the surface, show relatively reduced values of stiffness, and filaments close to the surface displayed rather great hardness.

He Huang and co-workers [105] studied the influence of thickness of tape on the characteristics of silver-sheathed 122 superconducting tapes. The $H_v$ of the tapes were gauged on the polished cross-section with a duration of 10 s and with 50 g load. Around 30 positions were gauged for each specimen by a Vickers hardness tester. The results showed that the mean $H_v$ values rise with reducing the thickness of tapes until the tapes rolled to 0.5 mm. The relationship between $H_v$ and $J_c$ was studied, and the results showed that $H_v$ values of 0.4 mm tapes is equivalent to that of 0.5 mm tapes ($H_v = 0.88$GPa), however the values of $J_c$ for tapes with 0.4 mm thickness are greater than that of for tapes with 0.5 mm thickness, indicating the saturation of the core density inside the Ag sheath. Shifa Liu et al. [106] fabricated

7-filamentary 122 tapes and wires via HIP. By performing Vickers measurements using the Wilson 402MVD tester with 10 s duration and 25 g load on well-polished samples, the authors assessed the mechanical property of 7-filamentary 122 tapes and wires. For IBSc, superconducting cores mass density can be estimated via Vickers hardness. Great $H_v$ designates a dense IBSc phase and therefore is advantageous to the transport performances. The average value of $H_v$ is above 1.96 GPa for 7-filamentary 122 wire. Such a value is higher than that obtained in Refs. [104, 105]. This indicates a significant enhancement in grain conductivity achieved by the HIP process.

## 7 Conclusion

The implementation of superconducting materials in different applications requires a clear understanding and extensive studies of their mechanical properties. The mechanical property of material is affected by different factor such as the preparation process, degree of heat treatment temperature, doping effect. In bulk superconductors, generally improved mechanical behavior appeared with the effect of doping or additives. The extensive progress of alloys superconductor (such as Nb-Ti, $Nb_3Sn$, etc.), cuprates (REBCO or BSCCO), pnictides and $MgB_2$ wires and tapes open the way to wide-ranging applications needing a high magnetic field such cables, MRI, NMR, motors and generators and so on. These wire and tape types might achieve industrial performance levels for multi-applications. To outline the potential wire or tapes application, works on various mechanical properties is needed. Composite wires consist of a metal sheath tube, co-axial inner powder rod, which are wrapped into the space between the sheath tube and the rod. For wires and tapes fabrication, PIT process is one is the most common used processes due to its ease to scale up. Metal-sheathed superconducting tapes/wires are frequently made by the PIT method. Yet, sustained research and development centers in many countries yielded great achievement in the manufacture of wires and tapes by using other alternatives processes to further enhance their mechanical properties hence expand their deployment beyond what is economically feasible. Previous and current investigations on the mechanical properties of different types of superconductors, even if elementary, should be considered as the basis for further improvements in the future in view of better control of the material.

## References

1. P. Mukherjee, V.V. Rao, Design and development of high temperature superconducting magnetic energy storage for power applications—a review. Phys. C: Supercond. Appl. **563**, 67–73 (2019)
2. K.S. Haran, S. Kalsi, T. Arndt, H. Karmaker, R. Badcock, B. Buckley, E.W. Stautner,

High power density superconducting rotating machines—development status and technology roadmap. Supercond. Sci. Technol. **30**(12), 123002
3. S. Zhao, S. Withington, D.J. Goldie, C.N. Thomas, Electromagnetic models for multilayer superconducting transmission lines. Supercond. Sci. Technol. **31**(8), 085012
4. I. Faridmehr, M.H. Osman, A.B. Adnan, A.F. Nejad, R. Hodjati, M. Azimi, Correlation between engineering stress–strain and true stress–strain curve. Am. J. Civ. Eng. Archit. **2**(1), 53–59 (2014)
5. J. Hay, Introduction to instrumented indentation testing. Exp. Tech. **33**(6), 66–72 (2009)
6. M.L. Palacio, B. Bhushan, Depth-sensing indentation of nanomaterials and nanostructures. Mater. Charact. **78**, 1–20 (2013)
7. S.R. Jian, G.J. Chen, W.M. Hsu, Mechanical properties of $Cu_2O$ thin films by nanoindentation. Materials **6**(10), 4505–4513 (2013)
8. W.C. Oliver, G.M. Pharr, An improved technique for determining hardness and elastic modulus using load and displacement sensing indentation experiments. J. Mater. Res. **7**(6), 1564–1583 (1992)
9. C. Ullner, A. Germak, H. Le Doussal, R. Morrell, T. Reich, W. Vandermeulen, Hardness testing on advanced technical ceramics. J. Eur. Ceram. Soc. **21**(4), 439–451 (2001)
10. G.E. Dieter, D.J. Bacon, *Mechanical Metallurgy*, vol. 3 (McGraw-Hill, New York, 1976)
11. B. Kaur, M. Bhat, F. Licci, R. Kumar, P.N. Kotru, K.K. Bamzai, Effect of 50 MeV Li3+ ion irradiation on mechanical characteristics of pure and Ga–In substituted M-type strontium hexaferrite. Nucl. Instrum. Methods Phys. Res., Sect. B **222**(1–2), 175–186 (2004)
12. O. Uzun, T. Karaaslan, M. Keskin, Hardness evaluation of Al–12Si–0.5 Sb melt–spun ribbons. J. Alloys Compd. **358**(1–2), 104–111 (2003)
13. E. Martinez, J. Romero, A. Lousa, J. Esteve, Nanoindentation stress–strain curves as a method for thin-film complete mechanical characterization: application to nanometric CrN/Cr multilayer coatings. Appl. Phys. A **77**(3), 419–426 (2003)
14. U. Kölemen, Analysis of ISE in microhardness measurements of bulk MgB2 superconductors using different models. J. Alloy. Compd. **425**(1–2), 429–435 (2006)
15. O. Uzun, T.U.N.C.A.Y. Karaaslan, M. Gogebakan, M.U.S.T.A.F.A. Keskin, Hardness and microstructural characteristics of rapidly solidified Al–8–16 wt.% Si alloys. J. Alloys Compd. **376**(1–2), 149–157
16. J. Gong, J. Wu, Z. Guan, Examination of the indentation size effect in low-load Vickers hardness testing of ceramics. J. Eur. Ceram. Soc. **19**(15), 2625–2631 (1999)
17. J. Gong, Z. Zhao, Z. Guan, H. Miao, Load-dependence of Knoop hardness of $Al_2O_3$–TiC composites. J. Eur. Ceram. Soc. **20**(12), 1895–1900 (2000)
18. J. Gong, Y. Li, An energy-balance analysis for the size effect in low-load hardness testing. J. Mater. Sci. **35**(1), 209–213 (2000)
19. M.B. Turkoz, S. Nezir, O. Ozturk, E. Asikuzun, G. Yildirim, C. Terzioglu, A. Varilci, Experimental and theoretical approaches on mechanical evaluation of Y123 system by Lu addition. J. Mater. Sci.: Mater. Electron. **24**(7), 2414–2421 (2013)
20. A. Leenders, M. Mich, H.C. Freyhard, Influence of thermal cycling on the mechanical properties of VGF melt-textured YBCO. Phys. C **279**(3–4), 173–180 (1997)
21. R. Awad, A.I. Abou Aly, M. Kamal, M. Anas, Mechanical properties of (Cu 0.5 Tl 0.5)-1223 substituted by Pr. J. Supercond. Novel Magn. **24**(6), 1947–1956
22. H. Li, R.C. Bradt, The microhardness indentation load/size effect in rutile and cassiterite single crystals. J. Mater. Sci. **28**(4), 917–926 (1993)
23. L. Sidjanin, D. Rajnovic, J. Ranogajec, E. Molnar, Measurement of Vickers hardness on ceramic floor tiles. J. Eur. Ceram. Soc. **27**(2–3), 1767–1773 (2007)
24. B.R. Lawn, V.R. Howes, Elastic recovery at hardness indentations. J. Mater. Sci. **16**(10), 2745–2752 (1981)
25. A. Toplu, I. Karaca, U. Kölemen, Calculation of true hardness value of Zn added (BiPb) SrCaCuO superconductor by different models. Ceram. Int. **41**(1), 953–960 (2015)
26. H. Li, R.C. Bradt, The effect of indentation-induced cracking on the apparent microhardness. J. Mater. Sci. **31**(4), 1065–1070 (1996)

27. H. Li, Y.H. Han, R.C. Bradt, Knoop microhardness of single crystal sulphur. J. Mater. Sci. **29**(21), 5641–5645 (1994)
28. G. Myneni, *Mechanical Properties of High Purity Niobium-Novel Measurements* (No. JLAB-ACC-04-01; DOE/ER/40150-2617). Thomas Jefferson National Accelerator Facility, Newport News, VA (US)
29. H. Jiang, T.R. Bieler, C. Compton, T.L. Grimm, *Proceedings of the 12th International Workshop on RF Superconductivity* (Ithaca, New York, Cornell University, 2005)
30. A. Zamiri, F. Pourboghrat, H. Jiang, T.R. Bieler, F. Barlat, J. Brem, T.L. Grimm, On mechanical properties of the superconducting niobium. Mater. Sci. Eng. A **435**, 658–665 (2006)
31. R.M. Scanlan, A.P. Malozemoff, D.C. Larbalestier, Superconducting materials for large scale applications. Proc. IEEE **92**(10), 1639–1654 (2004)
32. M. Fischer, D. Joguet, G. Robin, L. Peltier, P. Laheurte, In situ elaboration of a binary Ti–26Nb alloy by selective laser melting of elemental titanium and niobium mixed powders. Mater. Sci. Eng. C **62**, 852–859 (2016)
33. G.P. Vedernikov, A.K. Shikov, L.V. Potanina, E.I. Plashkin, E.V. Nikulenkov, I.N. Gubkin, V.Y. Korpusov, Development of fine filament NbTi superconducting strands for magnet systems of fusion reactors. Phys. C **354**(1–4), 420–423 (2001)
34. H.C. Kanithi, P. Valaris, B.A. Zeitlin, A novel approach to make fine filament superconductors, in *Supercollider*, vol. 4 (Springer, Boston, MA, 1992), pp. 41–47
35. Z. Guo, W.H. Warnes, Mechanical behavior of fine filament Nb-Ti as a function of processing (composite superconductors). IEEE Trans. Appl. Supercond. **3**(1), 1022–1025 (1993)
36. H. Liu, Mechanical properties of Nb–Ti composite superconducting wires (1991)
37. A. Cremasco, W.R. Osorio, C.M. Freire, A. Garcia, R. Caram, Electrochemical corrosion behavior of a Ti–35Nb alloy for medical prostheses. Electrochim. Acta **53**(14), 4867–4874 (2008)
38. H. Yu, J.W. Levitan, J. Lu, Calibration of a superconducting transformer by measuring critical current of a NbTi Rutherford cable. Supercond. Sci. Technol. (2021)
39. A. M. Ferreira, M.A. Martorano, N.B. de Lima, A.F. Padilha, Effects of recovery and recrystallization on microstructure and texture during annealing of a cold deformed superconducting Nb-50 (wt.)% Ti alloy. J. Alloys Comps. **887**, 161334 (2021)
40. P.J. Lee, D.C. Larbalestier, Niobium-titanium superconducting wires: Nanostructures by extrusion and wiredrawing. Wire J. Int. (USA) **36**(2), 61–66 (2003)
41. A.M. Campbell, J.E. Evetts, Flux vortices and transport currents in type II superconductors. Adv. Phys. **50**(8), 1249–1449 (2001)
42. A. Ballarino, L. Bottura, Targets for R&D on Nb 3 Sn conductor for high energy physics. IEEE Trans. Appl. Supercond. **25**(3), 1–6 (2015)
43. Rossi, L. (2011). LHC upgrade plans: options and strategy (No. IPAC-2011-TUYA02, p. TUYA02)
44. F. Savary, M. Bajko, B. Bordini, L. Bottura, L. Fiscarelli, J. Fleiter, A.V. Zlobin, Progress on the development of the $Nb_3Sn$ 11T dipole for the high luminosity upgrade of LHC. IEEE Trans. Appl. Supercond. **27**(4), 1–5 (2017)
45. J.L.R. Fernández, J.C. Perez, S.F. Troitino, M. Guinchard, P. Grosclaude, M.D. Crouvizier, F. Savary, Characterization of the mechanical properties of $Nb_3Sn$ Coils. IEEE Trans. Appl. Supercond. **29**(5), 1–5 (2019)
46. P. Ebermann, J. Bernardi, J. Fleiter, F. Lackner, F. Meuter, M. Pieler, E. Eisterer, Irreversible degradation of $Nb_3Sn$ Rutherford cables due to transverse compressive stress at room temperature. Supercond. Sci. Technol. **31**(6), 065009 (2018)
47. E. Barzi, C. Franceschelli, I. Novitski, F. Sartori, A.V. Zlobin, Measurements and modeling of mechanical properties of nb 3 sn strands, cables, and coils. IEEE Trans. Appl. Supercond. **29**(5), 1–8 (2019)
48. B.A. Glowacki, Niobium aluminide as a source of high-current superconductors. Intermetallics **7**(2), 117–140 (1999)
49. D.R. Bloyer, K.V. Rao, R.O. Ritchie, Resistance-curve toughening in ductile/brittle layered structures: behaviour in Nb/$Nb_3Al$ laminates. Mater. Sci. Eng. A **216**(1–2), 80–90 (1996)

50. C.D. Bencher, A. Sakaida, K.V. Rao, R.O. Ritchie, Toughening mechanisms in ductile niobium-reinforced niobium aluminide (Nb/Nb 3 Al) in situ composites. Metall. and Mater. Trans. A. **26**(8), 2027–2033 (1995)
51. K.S. Chan, Alloying effects on fracture mechanisms in Nb-based intermetallic in-situ composites. Mater. Sci. Eng., A **329**, 513–522 (2002)
52. L.M. Peng, Synthesis and mechanical properties of niobium aluminide-based composites. Mater. Sci. Eng., A **480**(1–2), 232–236 (2008)
53. Y. Slimani, M.A. Almessiere, E. Hannachi, A. Baykal, A. Manikandan, M. Mumtaz, F.B. Azzouz, Influence of $WO_3$ nanowires on structural, morphological and flux pinning ability of $YBa_2Cu_3Oy$ superconductor. Ceram. Int. **45**(2), 2621–2628 (2019)
54. E. Hannachi, Y. Slimani, F.B. Azzouz, A.H.M.E.T. Ekicibil, Higher intra-granular and inter-granular performances of YBCO superconductor with TiO2 nano-sized particles addition. Ceram. Int. **44**(15), 18836–18843 (2018)
55. E. Hannachi, M.A. Almessiere, Y. Slimani, A. Baykal, F.B. Azzouz, AC susceptibility investigation of YBCO superconductor added by carbon nanotubes. J. Alloys Compd. **812**, 152150 (2020)
56. R. Algarni, M.A. Almessiere, Y. Slimani, E. Hannachi, F.B. Azzouz, Enhanced critical current density and flux pinning traits with $Dy_2O_3$ nanoparticles added to $YBa_2Cu_3O_7$-d superconductor. J. Alloys Compd. **852**, 157019 (2021)
57. Y. Slimani, E. Hannachi, A.H.M.E.T. Ekicibil, M.A. Almessiere, F.B. Azzouz, Investigation of the impact of nano-sized wires and particles $TiO_2$ on Y-123 superconductor performance. J. Alloy. Compd. **781**, 664–673 (2019)
58. S.A. Alotaibi, Y. Slimani, E. Hannachi, M.A. Almessiere, G. Yasin, F.O. Al-qwairi, F.B. Azzouz, Intergranular properties of polycrystalline $YBa_2Cu_3O_7$—δ superconductor added with nanoparticles of $WO_3$ and $BaTiO_3$ as artificial pinning centers. Ceram. Int. (2021)
59. N. El Ghouch, R. Al-Oweini, K. Habanjar, R. Awad, Comparative study on the effect of adding two transition-metal-substituted polyoxometalates on the mechanical properties of the (Bi, Pb)-2223 superconducting phase. J. Phys. Chem. Solids **151**, 109807 (2021)
60. N. Loudhaief, H. Labiadh, E. Hannachi, M. Zouaoui, M.B. Salem, Synthesis of CdS nanoparticles by hydrothermal method and their effects on the electrical properties of Bi-based superconductors. J. Supercond. Novel Magn. **31**(8), 2305–2312 (2018)
61. S.M. Khalil, Enhancement of superconducting and mechanical properties in BSCCO with Pb additions. J. Phys. Chem. Solids **62**(3), 457–466 (2001)
62. Anas, M. (2020). The effect of $PbF_2$ doping on the structural, electrical and mechanical properties of (Bi, Pb)–2223 superconductor. Chem. Phys. Lett. **742**, 137033
63. T. Nakashima, K. Yamazaki, S. Kobayashi, T. Kagiyama, M. Kikuchi, S. Takeda, K. Osamura, Drastic improvement in mechanical properties of DI-BSCCO wire with novel lamination material. IEEE Trans. Appl. Supercond. **25**(3), 1–5 (2015)
64. K. Osamura, S. Machiya, T. Kawasaki, S. Harjo, T. Kato, S. Kobayashi, G. Osabe, Mechanical—electromagnetic property of stainless sheet laminated BSCCO–2223 wires. Mater. Res. Express **6**(2), 026001 (2018)
65. A. Godeke, D.V. Abraimov, E. Arroyo, N. Barret, M.D. Bird, A. Francis, J.M. White, A feasibility study of high-strength Bi-2223 conductor for high-field solenoids. Supercond. Sci. Technol. **30**(3), 035011 (2017)
66. Z.H. Mao, H. Jin, J.G. Qin, F. Liu, C. Dai, Q.B. Hao, C.S. Li, Axial tensile stress–strain characterization of Bi-2212 round wire with different heat treatments. IEEE Trans. Appl. Supercond. **27**(6), 1–5 (2017)
67. Y. Yoshino, A. Iwabuchi, K. Noto, N. Sakai, M. Murakami, Vickers hardness properties of YBCO bulk superconductor at cryogenic temperatures. Phys. C **357**, 796–798 (2001)
68. S.V. Lubenets, V.D. Natsik, L.S. Fomenko, H.J. Kaufmann, V.S. Bobrov, A.N. Izotov, Influence of oxygen content and structural defects on low-temperature mechanical properties of high-temperature superconducting single crystals and ceramics. Low Temp. Phys. **23**(8), 678–683 (1997)

69. N. Güçlü, U. Kölemen, O. Uzun, S.E.L.A.H.A.T.T.İN. Çelebi, Work of indentation approach for investigation of mechanical properties of YBCO bulk superconductor at cryogenic temperatures. Phys. C **433**(1–2), 115–122 (2005)
70. A. Matsumuro, K. Kasumi, U. Mizutani, M. Senoo, Superconducting and mechanical properties of YBCO/Ag composites fabricated at high pressures up to 5.4 GPa. J. Mater. Sci. **26**(3), 737–742
71. A.K. Najem, Physical and electrochemical properties of (Bi, Pb)-2223 prepared at different pressures (2020)
72. U. Kölemen, S.E.L.A.H.A.T.T.İN. Çelebi, Y. Yoshino, A. Öztürk, Mechanical properties of YBCO and YBCO+ ZnO polycrystalline superconductors using Vickers hardness test at cryogenic temperatures. Phys. C **406**(1–2), 20–26 (2004)
73. T.A.K.U.Y.A. Takematsu, R.U.X.I.N. Hu, T.O.M.O.A.K.I. Takao, Y.O.S.H.I.N.O.R.I. Yanagisawa, H. Nakagome, D. Uglietti, H. Maeda, Degradation of the performance of a YBCO-coated conductor double pancake coil due to epoxy impregnation. Phys. C: Supercond. Appl. **470**(17–18), 674–677 (2010)
74. Y. Yanagisawa, H. Nakagome, T. Takematsu, T. Takao, N. Sato, M. Takahashi, H. Maeda, Remarkable weakness against cleavage stress for YBCO-coated conductors and its effect on the YBCO coil performance. Phys. C: Supercond. Appl. **471**(15–16), 480–485 (2011)
75. U.P. Trociewitz, M. Dalban-Canassy, M. Hannion, D.K. Hilton, J. Jaroszynski, P. Noyes, D.C. Larbalestier, 35.4 T field generated using a layer-wound superconducting coil made of (RE) Ba2Cu3O7−x (RE= rare earth) coated conductor. Appl. Phys. Lett. **99**(20), 202506 (2011)
76. S. Hahn, D.K. Park, J. Bascuñán, Y. Iwasa, HTS pancake coils without turn-to-turn insulation. IEEE Trans. Appl. Supercond. **21**(3), 1592–1595 (2010)
77. S. Matsumoto, T. Kiyoshi, A. Otsuka, M. Hamada, H. Maeda, Y. Yanagisawa, H. Suematsu, Generation of 24 T at 4.2 K using a layer-wound GdBCO insert coil with $Nb_3Sn$ and Nb–Ti external magnetic field coils. Supercond. Sci. Technol. **25**(2), 025017 (2012)
78. M. Tomita, M. Murakami, K. Yoneda, Improvements in the mechanical properties of bulk YBCO superconductors with carbon fibre fabrics. Supercond. Sci. Technol. **15**(5), 803 (2002)
79. G. Wang, H. Ding, R. He, Z. Huang, H. Liu, J. Qin, Y. Tan, A new method for avoiding critical current degradation of YBCO coils using ice impregnation. Supercond. Sci. Technol. **32**(10), 105011 (2019)
80. M. Anas, S. Ebrahim, I.G. Eldeen, R. Awad, A.I. Abou-Aly, Effect of single and multi-wall carbon nanotubes on the mechanical properties of Gd-123 superconducting phase. Chem. Phys. Lett. **686**, 34–43 (2017)
81. N. Hameed, S.P. Thomas, R. Abraham, S. Thomas, Morphology and contact angle studies of poly (styrene-co-acrylonitrile) modified epoxy resin blends and their glass fibre reinforced composites. Express Polym Lett **1**(6), 345–355 (2007)
82. S. Yu, P. Hing, X. Hu, Dielectric properties of polystyrene–aluminum-nitride composites. J. Appl. Phys. **88**(1), 398–404 (2000)
83. C.B. Yoon, S.H. Lee, S.M. Lee, Y.H. Koh, H.E. Kim, K.W. Lee, Piezoelectric multilayer ceramic/polymer composite transducer with 2–2 connectivity. J. Am. Ceram. Soc. **89**(8), 2509–2513 (2006)
84. R. Abraham, P. Thomas, S., Kuryan, S., Issac, J., Nandakumar, K., & Thomas, S., Structural and mechanical properties of YBCO-polystyrene composites. J. Appl. Polym. Sci. **118**(2), 1027–1041 (2010)
85. A.I. Kupchishin, B.G. Taipova, N.A. Voronova, Study of the influence of filler on the mechanical properties of composites based on polyimide, in *IOP Conference Series: Materials Science and Engineering*, vol. 168, no. 1 (IOP Publishing, 2017), p. 012015
86. T. Hlásek, K.Y. Huang, J. Esnoz-Larraya, V. Plecháček, J. Durrell, I. Valiente-Blanco, D.A. Cardwell, Enhanced mechanical properties of single-domain YBCO bulk superconductors processed with artificial holes. IEEE Trans. Appl. Supercond. **29**(5), 1–4 (2019)
87. R. Cloots, T. Koutzarova, J.P. Mathieu, M. Ausloos, From RE-211 to RE-123. How to control the final microstructure of superconducting single-domains. Superconduct. Sci. Technol. **18**(3), R9 (2004)

88. D.K. Namburi, K. Singh, K.Y. Huang, S. Neelakantan, J.H. Durrell, D.A. Cardwell, Improved mechanical properties through recycling of Y-Ba-Cu-O bulk superconductors. J. Eur. Ceram. Soc. **41**(6), 3480–3492 (2021)
89. J. Nagamatsu, N. Nakagawa, T. Muranaka, Y. Zenitani, J. Akimitsu, Superconductivity at 39 K in magnesium diboride. Nature **410**(6824), 63–64 (2001)
90. T. Machi, S. Shimura, N. Koshizuka, M. Murakami, Fabrication of MgB2 superconducting wire by in situ PIT method. Phys. C **392**, 1039–1042 (2003)
91. J.G. Noudem, Y. Xing, P. Bernstein, R. Retoux, M. Higuchi, S.S. Arvapalli, M. Murakami, Improvement of critical current density of $MgB_2$ bulk superconductor processed by Spark Plasma Sintering. J. Am. Ceram. Soc. **103**(11), 6169–6175 (2020)
92. G. Giunchi, T. Cavallin, P. Bassani, S. Guicciardi, The mechanical properties of the $MgB_2$ bulk materials obtained by reactive liquid Mg infiltration, in *AIP Conference Proceedings*, vol. 986, no. 1 (American Institute of Physics, 2008)
93. N. Kumar, S. Das, C. Bernhard, G.D. Varma, Effect of graphene oxide doping on superconducting properties of bulk $MgB_2$. Supercond. Sci. Technol. **26**(9), 095008 (2013)
94. M. Muralidhar, K. Inoue, M.R. Koblischka, A. Murakami, M. Murakami, Effects of silver addition on critical current densities and mechanical properties in bulk $MgB_2$. Adv. Eng. Mater. **17**(6), 831–838 (2015)
95. K.M. Elsabawy, Narrow range of hafnium doping for promoted mechanical properties and critical current density (Jc) values of Mg 1–x Hf x B 2 superconductor. J. Supercond. Novel Magn. **24**(6), 1853–1861 (2011)
96. N. Kaya, Ş. Çavdar, Ö. Öztürk, H. Ada, H. Koralay, Investigation of microhardness properties of the multi-walled carbon nanotube additive $MgB_2$ structure by using the vickers method. Cryogenics **116**, 103295 (2021)
97. A.B. Abrahamsen, D. Liu, N. Magnusson, A. Thomas, Z. Azar, E. Stehouwer, H. Polinder, Comparison of levelized cost of energy of superconducting direct drive generators for a 10-MW offshore wind turbine. IEEE Trans. Appl. Supercond. **28**(4), 1–5 (2018)
98. P. Kováč, I. Hušek, T. Melišek, L. Kopera, M. Reissner, Stainless steel reinforced multi-core $MgB_2$ wire subjected to variable deformations, heat treatments and mechanical stressing. Supercond. Sci. Technol. **23**(6), 065010 (2010).
99. P. Kovac, L. Kopera, Electromechanical properties of filamentary $MgB_2$ wires. IEEE Trans. Appl. Supercond. **22**(1), 8400106–8400106 (2011)
100. I. Hušek, P. Kováč, Mechanical properties, interface reactions and transport current densities of multi-core $MgB_2$/Ti/Cu/SS wire. Supercond. Sci. Technol. **23**(7), 075012 (2010)
101. A.E. Ozmetin, O. Sahin, E. Ongun, M. Kuru, Mechanical characterization of $MgB_2$ thin films using nanoindentation technique. J. Alloy. Compd. **619**, 262–266 (2015)
102. H. Hosono, Layered iron pnictide superconductors: discovery and current status. J. Phys. Soc. Jpn. **77**(Suppl. C), 1–8 (2008)
103. C. Yao, H. Lin, Q. Zhang, X. Zhang, D. Wang, C. Dong, K. Watanabe, Critical current density and microstructure of iron sheathed multifilamentary Sr1−xKxFe2As2/Ag composite conductors. J. Appl. Phys. **118**(20), 203909 (2015)
104. G. Xu, X. Zhang, C. Yao, H. Huang, Y. Zhu, L. Li, Y. Ma, Effects of different directional rolling on the fabrication of 7-filament Ba1-xKxFe2As2 tapes. Phys. C: Supercond. Appl. **561**, 30–34 (2019)
105. H. Huang, C. Yao, Y. Zhu, X. Zhang, C. Dong, D. Wang, Y. Ma, Influences of tape thickness on the properties of Ag-Sheathed Sr 1–x K x Fe 2 As 2 superconducting tapes. IEEE Trans. Appl. Supercond. **28**(4), 1–5 (2017)
106. S. Liu, C. Yao, H. Huang, C. Dong, W. Guo, Z. Cheng, Y. Ma, Enhancing transport performance in 7-filamentary Ba0. 6K0. 4Fe2As2 wires and tapes via hot isostatic pressing. Phys. C: Supercond. Appl. **585**, 1353870 (2021)